A new analytical edge spread function fitting model for modulation transfer function measurement

Tiecheng Li (李铁成), Huajun Feng (冯华君)*, and Zhihai Xu (徐之海)

State Key Laboratory of Modern Optical Instrumentation, Zhejiang University, Hangzhou 310027, China

**Corresponding author: fenghj@zju.edu.cn*

Received August 24, 2010; accepted October 21, 2010; posted online February 21, 2011

We propose a new analytical edge spread function (ESF) fitting model to measure the modulation transfer function (MTF). The ESF data obtained from a slanted-edge image are fitted to our model through the non-linear least squares (NLLSQ) method. The differentiation of the ESF yields the line spread function (LSF), the Fourier transform of which gives the profile of two-dimensional MTF. Compared with the previous methods, the MTF estimate determined by our method conforms more closely to the reference. A practical application of our MTF measurement in degraded image restoration also validates the accuracy of our model.

OCIS codes: 110.4100, 110.2960, 100.2000, 100.1830.
doi: 10.3788/COL201109.031101.

Modulation transfer function (MTF) has been widely used to characterize the spatial frequency response of a linear and space-invariant imaging system. A straightforward approach to measuring the MTF involves imaging a known input, such as a point or a line source, to produce the point spread function (PSF) and the line spread function (LSF), respectively[1,2]. However, the use of a point or a line source requires precise fabrication and high exposure. Thus, an edge source is imaged to yield the edge spread function (ESF) instead, which can then be differentiated to obtain LSF[3−12].

ESF measurement can be done in a number of ways and is the subject of this letter. Bentzen[13] has fitted a model such as the error function to the ESF data, which can be differentiated analytically to produce a Gaussian-shaped LSF. Yin *et al.*[14] have fitted the LSF data to a model that is given by the sum of a Gaussian (for the central part) and an exponential (for the tail part) functions. Boone *et al.*[15] have extended the technique of Yin *et al.* in order for the model to be used to measure the ESF as well. Tzannes *et al.*[16] have used the sum of Fermi functions to achieve the desired fit to the ESF data. All of these models are based on the fact that they have similar shapes with a typical ESF, which implies that they lack in analytical derivation.

In this letter, we propose a new analytical ESF fitting model to measure MTF. Unlike the previous models, our proposed model is derived from the scalar diffraction theory. By fitting the ESF data to analytical expression, the LSF and MTF can be easily calculated from the ESF fitting coefficients.

When the object illumination is incoherent, the image intensity distribution is calculated as[17]

$$I_i(x) = \int_{-\infty}^{\infty} I_o(\xi) a^2 \sin c^2 \left[\frac{\pi a(x + m\xi)}{(1+m)\lambda f} \right] \mathrm{d}\xi, \quad (1)$$

where $I_o(\xi)$ is the intensity distribution transmitted by the object; a is the diameter of the aperture; m is the magnification of the system; λ is the mean wavelength of the light source; f is the focal length of the system.

Thus, the intensity image of a step object (edge along the y axis) is given by

$$\mathrm{ESF}(x,k) = \frac{\pi}{2} + \mathrm{Si}(Akx) + \frac{\cos(Akx) - 1}{Akx}, \quad (2)$$

where $A = \frac{a}{(1+m)f}$ is a constant; $k = \frac{2\pi}{\lambda}$ is the wave number; $\mathrm{Si}(x) = \int_0^x \frac{\sin t}{t} \mathrm{d}t$ is the sine integral function.

In the case of polychromatic irradiation, the effective ESF is obtained[18]

$$\mathrm{ESF}(x) = \int S(\lambda) D(\lambda) \mathrm{ESF}(x,\lambda) \mathrm{d}\lambda, \quad (3)$$

where $S(\lambda)$ is the spectral energy of the incident radiation and $D(\lambda)$ is the photocathode sensitivity.

For simplicity, we suppose that the imaging system has a constant spectral energy and photocathode sensitivity. Thus, substituting Eq. (2) in Eq. (3), we derive

$$\begin{aligned} \mathrm{ESF}(x) &= \int_{\lambda_2}^{\lambda_1} \mathrm{ESF}(x,\lambda) \mathrm{d}\lambda = \int_{k_2}^{k_1} \mathrm{ESF}(x,k) \Big(-\frac{2\pi}{k^2} \Big) \mathrm{d}k \\ &= (-2\pi) \left[\frac{-\pi}{2k} + \frac{Ax\mathrm{Ci}(Akx)}{2} - \frac{\sin(Akx)}{2k} \right. \\ &\quad \left. - \frac{\mathrm{Si}(Akx)}{k} + \frac{1 - \cos(Akx)}{2Ak^2 x} \right] \Bigg|_{k_2}^{k_1}, \end{aligned} \quad (4)$$

where $k_1 = \frac{2\pi}{\lambda_1} = \frac{2\pi}{780}$ and $k_2 = \frac{2\pi}{\lambda_2} = \frac{2\pi}{380}$ correspond to the upper and lower limits of the visible spectrum (380−780 nm), respectively.

As most ESFs are not well behaved and symmetric about the midpoint of the edge, a summation of three ESF functions is used to achieve the desired fit. Thus, the resulting ESF fitting model is given by

$$E(x) = d + \sum_{i=1}^{3} a_i \mathrm{ESF}\Big(\frac{x - b_i}{c_i} \Big), \quad (5)$$

where d, a_i, b_i, and c_i are constants.

The ESF data obtained from the slanted-edge image are fitted by means of the non-linear least squares (NLLSQ) method.

The next step is to differentiate the ESF to arrive at the LSF. Substituting Eq. (4) in Eq. (5), we get

$$L(x) = \frac{\mathrm{d}E(x)}{\mathrm{d}x} = \sum_{i=1}^{3} a_i \frac{\mathrm{dESF}(\frac{x-b_i}{c_i})}{\mathrm{d}\frac{x-b_i}{c_i}} \cdot \frac{\mathrm{d}\frac{x-b_i}{c_i}}{\mathrm{d}x}$$
$$= (-2\pi) \sum_{i=1}^{3} \frac{a_i}{c_i} \left[\frac{A\mathrm{Ci}(Akx)}{2} - \frac{\sin(Akx)}{2kx} - \frac{1}{2Ak^2x^2} + \frac{\cos(Akx)}{2Ak^2x^2} \right] \Bigg|_{k_2, x=\frac{x-b_i}{c_i}}^{k_1}, \quad (6)$$

where $\mathrm{Ci}(x) = -\int_x^\infty \frac{\cos t}{t}\mathrm{d}t$ is the cosine integral function.

The one-dimensional (1D) discrete Fourier transform, (DFT) of the LSF is the profile through the center of the two-dimensional (2D) optical transfer function (OTF). The normalized modulus of the OTF is the MTF.

To compare our model with three previous models proposed by Bentzen, Yin *et al.*, and Tzannes *et al.*, we have designed and fabricated a doublet objective. The focal length is 387.7 mm and the F number is 15. Both the ESF and MTF can be obtained directly from Zemax, which can be used as a reference to evaluate the performance of different models.

Figure 1(a) shows the fitting results to the designed ESF by different models. None of the estimates is quite different from the others, indicating that all the four fitting models have similar performances. The details of the top portion of the fitting results are plotted in Fig. 1(b). It can be noted that Bentzen's fitting result deviates from the reference more than the other models. Figure 1(c) shows the resulting MTFs derived from the ESFs in Fig. 1(a). To distinguish the fine differences among all of these models, we compute the errors between the estimates and the reference, which are plotted in Fig. 1(d). All of the errors lie between −0.025 and 0.02, and fluctuate according to the frequency.

Similarly, we compare our model with the slanted-edge method proposed by ISO 12233[19]. The designed PSF

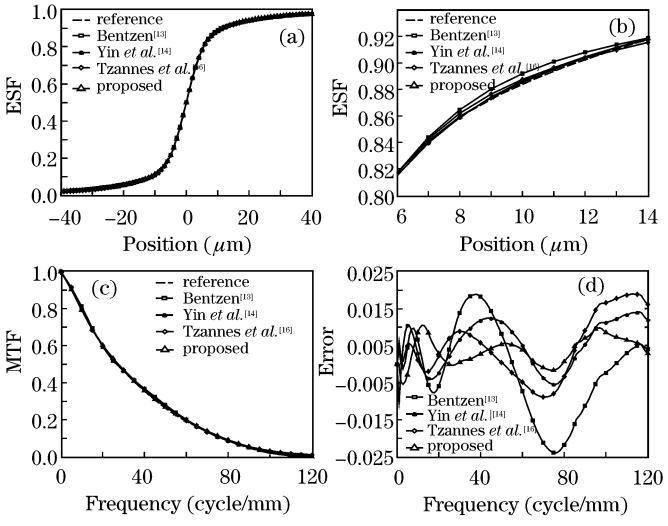

Fig. 1. (a) ESF fitting results by different models; (b) details of the top portion; (c) resulting MTF estimates; (d) errors between the estimates and the reference.

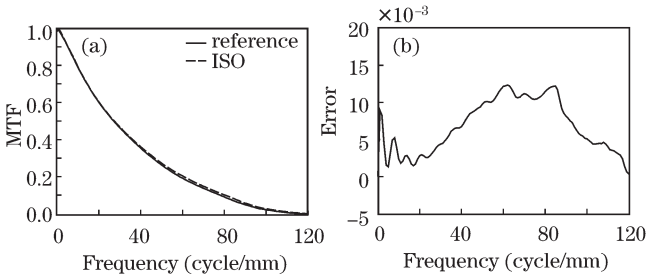

Fig. 2. (a) Comparison of the ISO estimate with the reference and (b) errors between the estimate and the reference.

Table 1. Max, Mean, and RMS Errors between the MTF Estimates and the Reference in the Absence of Noise

Method	Max Error	Mean Error	RMS Error
Bentzen[13]	0.0240	0.0098	0.0121
Yin *et al.*[14]	0.0141	0.0073	0.0085
Tzannes *et al.*[16]	0.0189	0.0077	0.0097
ISO	0.0123	0.0067	0.0076
Proposed	0.0105	0.0042	0.0052

is used to blur a perfect slanted-edge image. Applying the ISO method to the resulting degraded image, we arrive at an estimate of the MTF. Figure 2(a) shows the comparison of the ISO estimate with the MTF reference. The errors between the measured and designed values are plotted in Fig. 2(b). The ISO estimate is a little higher than the reference at almost all frequencies.

In Table 1, the errors in various methods are compared through the maximum, mean, and root mean square (RMS) errors. Among all the models, the estimate determined by Bentzen's model exhibits the largest error while that based on our model shows the lowest error. In the absence of noise, the estimate based on our model conforms more closely to the reference than that determined by the ISO method.

Noise deteriorates the imaging performance of an image sensor. Based on the central limit theorem, noise in digital images can be represented by Gaussian noise. Signal-to-noise ratio (SNR) is a measure used to quantify how much an image has been corrupted by noise. The SNR of a noisy slanted-edge image is defined in decibels[8,9]:

$$\mathrm{SNR} = 20 \log \frac{2(D_\mathrm{b} - D_\mathrm{d})}{\sigma_\mathrm{b} + \sigma_\mathrm{d}}, \quad (7)$$

where D_b and D_d are the means of the bright and dark sides, respectively; σ_b and σ_d are the standard deviations of the bright and dark sides, respectively.

To evaluate the performance of our model in the presence of noise, Gaussian noise is added to a slanted-edge image. Figure 3(a) shows the MTF estimates obtained from the resulting noisy image with an SNR of 30 dB. It is noted that the ISO estimate fluctuates significantly over such frequency. The corresponding errors between the MTF estimates and the reference are shown in Table 2. In this case, the estimates based on our model maintain the lowest errors.

The MTF estimates under different levels of Gaussian

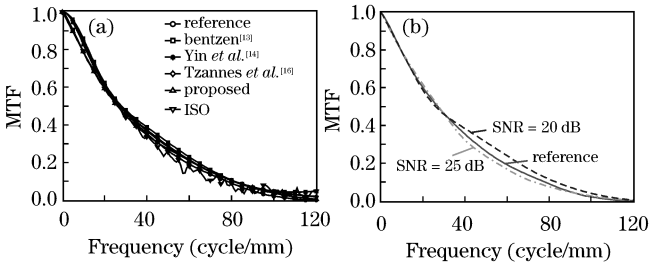

Fig. 3. (a) Performance evaluation under Gaussian noise (SNR = 30 dB) and (b) MTF estimates based on our model under different levels of Gaussian noise (SNR = 25 and 20 dB).

Table 2. Max, Mean, and RMS Errors between the MTF Estimates and the Reference under Different Levels of Gaussian Noise

Method	SNR (dB)	Max Error	Mean Error	RMS Error
Bentzen[13]	30	0.0696	0.0315	0.0345
	20	0.1773	0.0831	0.0910
Yin *et al.*[14]	30	0.0446	0.0194	0.0210
	20	0.1063	0.0409	0.0461
Tzannes *et al.*[16]	30	0.0578	0.0219	0.0245
	20	0.1374	0.0499	0.0558
ISO	30	0.0683	0.0193	0.0243
	20	0.2535	0.0836	0.0925
Proposed	30	0.0195	0.0114	0.0124
	25	0.0315	0.0140	0.0171
	20	0.0509	0.0218	0.0266

noise (SNR = 25 and 20 dB) based on our model are computed, and a comparison of the estimates with the reference is plotted in Fig. 3(b). As the noise increases, the estimate gradually deviates from the reference within the whole band of frequencies. As shown in Table 2, the resulting errors between the estimates and the reference increase with a decreasing SNR.

When SNR drops to 20 dB, as shown in Table 2, the MTF estimates in the various methods deviate much more from each other than before.

According to the abovementioned discussions, noise plays an important role in MTF measurement. In general, the more noise is added to the image, the more errors will be obtained from the calculation. Particularly, the measurement based on the ISO method is more sensitive to noise, which would contribute to a decrease at middle frequencies and an increase at high frequencies. In contrast, the MTF estimate based on our model is less affected by noise, implying that our model can work with a lower SNR. However, as noise increases, the MTF estimate based on our model finally inevitably fails.

Table 3 shows the time spent on the MTF calculation in various methods under different levels of Gaussian noise (SNR = ∞, 40, and 30 dB). As noise increases, the time increases as well. The time consumed by our model is much longer than the other models due to the model complexity. The time spent by the ISO method almost

Table 3. Time Spent on MTF Calculation in Various Methods under Different Levels of Gaussian Noise

Method	Time (s)		
	SNR = ∞	SNR = 40 dB	SNR = 30 dB
Bentzen[13]	0.422	0.453	3.188
Yin *et al.*[14]	0.250	0.271	2.234
Tzannes *et al.*[16]	0.063	0.078	4.000
ISO	0.982	0.985	1.047
Proposed	76.656	88.094	107.344

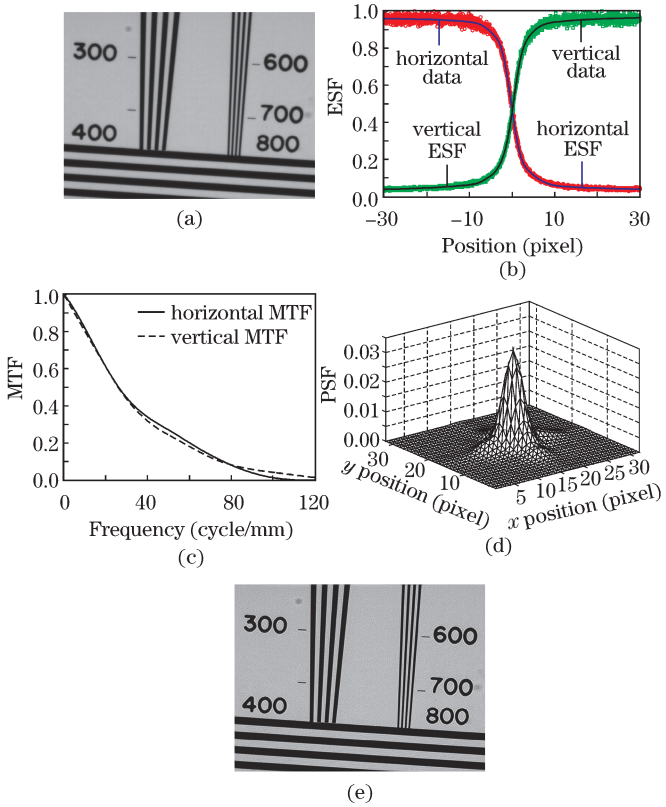

Fig. 4. (a) Resolution chart image; (b) ESF fitting results in both vertical and horizontal directions; (c) resulting MTF estimates; (d) resulting 2D PSF; (e) restoration result.

remains the same because it does not involve the fitting step.

Therefore, we need to choose between the fitting precision and running time. In the case of common MTF measurements, our model can provide a more accurate estimate; however, in the situation of quick real-time MTF measurements, the other methods can save much more time. Hence, the selection depends on the situation.

Our model has been used to estimate the MTF of a practical imaging system, which is composed of a charge-coupled device (CCD) camera with a sampling interval of 3.46 μm, and a doublet objective with a focal length of 387 mm. Figure 4(a) shows the resolution chart image acquired from the CCD camera. The fitting results to the ESF data in both vertical and horizontal directions are shown in Fig. 4(b). Figure 4(c) illustrates the calculated MTFs in both the vertical and horizontal directions. Both estimates are similar, except at some

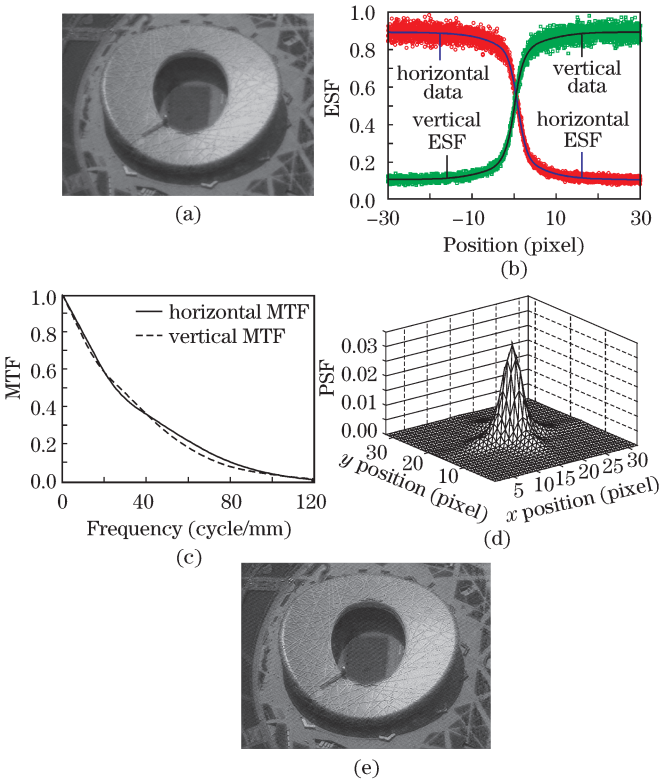

Fig. 5. (a) Remote image; (b) ESF fitting results in both vertical and horizontal directions; (c) resulting MTF estimates; (d) resulting 2D PSF; (e) restoration result.

Table 4. Objective Quality Assessment for Resolution Chart and Remote Images

Metrics	Resolution Chart Image		Remote Image	
	Degraded	Restored	Degraded	Restored
GMG	0.0183	0.0272	0.0202	0.0709
LS	0.0570	0.1066	0.0892	0.3285

high frequencies, indicating that the 2D OTF is nearly symmetric. 1D OTFs in both vertical and horizontal directions correspond to the Fourier transform of LSF (x) and LSF (y), respectively, which are combined as a vector product to create a 2D PSF[5,9]

$$\mathrm{PSF}(x,y) = \mathrm{LSF}(x) \otimes \mathrm{LSF}(y). \tag{8}$$

Figure 4(d) shows the resulting 2D PSF, which can be used to reconstruct the deteriorated images. Figure 4(e) shows the restoration result of the blurred resolution chart image. It is noted that details at high spatial frequencies can be seen more clearly. Meanwhile, the noise in the background has also been unavoidably amplified.

Similar to the resolution chart image, our method has been utilized to measure the MTF of a remote image shown in Fig. 5(a). The same deconvolution procedure has been performed, and Fig. 5(e) shows the corresponding restoration result. It is apparent that nest structures barely visible in the raw image can be identified more easily in the restored image.

Gray mean gradients (GMGs) and Laplacian summation (LS) are two of the most common no-reference objective image quality metrics[20]. A larger GMG or LS value means better image quality. In Table 4, both the resolution chart and remote images are assessed by the abovementioned measures. Both GMG and LS values increase after deconvolution, indicating that the image quality has been improved. The restoration result not only validates the MTF estimate calculated by our method but also demonstrates a practical application for our MTF measurement.

In conclusion, we propose a novel analytical fitting model for MTF measurement. Compared with the previous methods, the MTF estimates based on our method show the lowest error with respect to the reference, which are then used to restore degraded images via deconvolution. The results validate the accuracy of our model. Future research may focus on how to improve our algorithm to suit real-time MTF measurement and compensation.

This work was supported by the National Natural Science Foundation of China (No. 60977010), the National Key Basic Research and Development Program of China (No. 2009CB724006), the National High Technology Research and Development Program of China (No. 2009AA12Z108), and the Innovation Foundation of China Aerospace Science and Technology Corporation.

References

1. T. Choi, "IKONOS satellite on orbit modulation transfer function (MTF) measurement using edge and pulse method", MS. Thesis (South Dakota State University, 2002).
2. J. T. Olson, R. L. Espinola, and E. L. Jacobs, Opt. Eng. **46,** 016403 (2007).
3. S. E. Reichenbach, S. K. Park, and R. Narayanswamy, Opt. Eng. **30,** 170 (1991).
4. E. Samei, M. J. Flynn, and D. A. Reimann, Med. Phys. **25,** 102 (1998).
5. J. J. Shea, J. Electron. Imag. **8,** 196 (1999).
6. P. B. Greer and T. van Doorn, Med. Phys. **27,** 2048 (2000).
7. A.-K. Carton, D. Vandenbroucke, L. Struye, A. D. A. Maidment, Y.-H. Kao, M. Albert, H. Bosmans, and G. Marchal, Med. Phys. **32,** 1684 (2005).
8. S. Lashansky, S. Mansbach, M. Berger, T. Karasik, and M. Bin-Nun, Proc. SPIE **6941,** 69410Z (2008).
9. H. Hwang, Y.-W. Choi, S. Kwak, M. Kim, and W. Park, Proc. SPIE **7109,** 710905 (2008).
10. T. Li, H. Feng, Z. Xu, X. Li, Z. Cen, and Q. Li, Proc. SPIE **7498,** 74981H (2009).
11. F. Viallefont-Robinet and D. Léger, Opt. Express **18,** 3531 (2010).
12. T. Li, X. Tao, H. Feng, and Z. Xu, Acta Opt. Sin. (in Chinese) **30,** 2891 (2010).
13. S. M. Bentzen, Med. Phys. **10,** 579 (1983).
14. F. Yin, M. L. Giger, and K. Doi, Med. Phys. **17,** 962 (1990).
15. J. M. Boone and J. A. Seibert, Med. Phys. **21,** 1541 (1994).
16. A. P. Tzannes and J. M. Mooney, Opt. Eng. **34,** 1808 (1995).
17. P. S. Considine, J. Opt. Soc. Am. A **56,** 1001 (1966).
18. O. P. Nijhawan, S. K. Gupta, and R. Hradaynath, Appl. Opt. **22,** 2453 (1983).
19. International Organization for Standardization, ISO 12233:2000, Photography electronic still-picture cameras resolution measurements (2000).
20. W. Liu, "The research on restoration algorithm of motion blur image and its realization", PhD. Thesis (Changchun Institute of Optics, Fine Mechanics and Physics, 2005).